

^aPSE Division and ^cBESE Division, King Abdullah University of Science and Technology (KAUST), Thuwal, Kingdom of Saudi Arabia; ^bBioNEM Lab, Department of Experimental and Clinical Medicine, University Magna Graecia of Catanzaro, Catanzaro, Italy; ^dNanostructures and ^eNanochemistry, Istituto Italiano di Tecnologia, Genova, Italy; ^cCellular and Molecular Pathophysiology Laboratory, Department of Surgical and Oncological Sciences, University of Palermo, Palermo, Italy; ^fLaboratory for Experimental Oncology and Radiology (LEXOR), Center for Experimental Molecular Medicine (CEMM), Academic Medical Center (AMC), University of Amsterdam, Amsterdam, The Netherlands; ^hDepartment of Microbiology Tumor and Cell Biology (MTC), Karolinska Institute, Stockholm, Sweden; ⁱTumor Immunology Lab, Dipartimento di Medicina Sperimentale e Clinica, Università Magna Graecia di Catanzaro, Catanzaro, Italy.

Correspondence: Enzo Di Fabrizio, PhD, King Abdullah University of Science and Technology (KAUST), PSE and BESE Divisions, Thuwal 23955-6900, Kingdom of Saudi Arabia. Telephone: 966-128084307; e-mail: enzo.difabrizio@kaust.edu.sa

Received June 11, 2014; accepted for publication August 12, 2014; first published online in *STEM CELLS EXPRESS* September 3, 2014.

© 2014 The Authors. *STEM CELLS* Published by Wiley Periodicals, Inc. on behalf of AlphaMed Press 1066-5099/2014/\$30.00/0

<http://dx.doi.org/10.1002/stem.1837>

This is an open access article under the terms of the Creative Commons Attribution License, which permits use, distribution and reproduction in any medium, provided the original work is properly cited.

Lipid Droplets: A New Player in Colorectal Cancer Stem Cells Unveiled by Spectroscopic Imaging

LUCA TIRINATO,^{a,b} CARLO LIBERALE,^{c,d} SIMONE DI FRANCO,^{e,f} PATRIZIO CANDELORO,^b ANTONINA BENFANTE,^e ROSANNA LA ROCCA,^d LISETTE POTZE,^f ROBERTO MAROTTA,^g ROBERTA RUFFILLI,^g VIJAYAKUMAR P. RAJAMANICKAM,^{c,d} MARIO MALERBA,^d FRANCESCO DE ANGELIS,^d ANDREA FALQUI,^{c,g} ENNIO CARBONE,^{h,i} MATILDE TODARO,^e JAN PAUL MEDEMA,^f GIORGIO STASSI,^e ENZO DI FABRIZIO^{a,b,c}

Key Words. Colorectal cancer stem cells • Lipid droplets • Wnt/ β -catenin pathway • Raman spectroscopy

ABSTRACT

The cancer stem cell (CSC) model is describing tumors as a hierarchical organized system and CSCs are suggested to be responsible for cancer recurrence after therapy. The identification of specific markers of CSCs is therefore of paramount importance. Here, we show that high levels of lipid droplets (LDs) are a distinctive mark of CSCs in colorectal (CR) cancer. This increased lipid content was clearly revealed by label-free Raman spectroscopy and it directly correlates with well-accepted CR-CSC markers as CD133 and Wnt pathway activity. By xenotransplantation experiments, we have finally demonstrated that CR-CSCs overexpressing LDs retain most tumorigenic potential. A relevant conceptual advance in this work is the demonstration that a cellular organelle, the LD, is a signature of CSCs, in addition to molecular markers. A further functional characterization of LDs could lead soon to design new target therapies against CR-CSCs. *STEM CELLS* 2015;33:35–44

INTRODUCTION

Colorectal (CR) cancer is one of the most frequent neoplasms and the second leading cause of cancer-related death in the Western world [1]. CR cancer normally originates from clonal expansion of a single intestinal stem or progenitor cell located at the bottom of the CR crypt [2, 3] that undergoes genetic and/or epigenetic alterations [4, 5]. Nevertheless, the hierarchical organization that is present in the crypts as well as the morphogenic signals that sustain this hierarchy appears to be maintained throughout tumor progression [6, 7]. In agreement, tumors have been shown to contain a hierarchy with a cancer stem cell (CSC) compartment at the apex [8]. Importantly, different studies have indicated that these CSCs are more resistant to therapy than differentiated tumor cells [9, 10]. For these reasons, CR-CSCs have been recognized as key components in CR carcinogenesis and recurrences [11–13]. This is why their identification and isolation becomes a crucial step to better understand the mechanisms that underlie their biological behavior [14]. To address this issue, one or more of the following in vitro analyses have been used so far: detection of CR-CSC markers, serial colony forming assays, and the

propagation as tumor spheres in stem cell culturing conditions [15, 16]. To prove the tumorigenic potential of the isolated CR-CSCs, it is then necessary to perform serial injections of the spheres into immune compromised mice [17]. Unfortunately, nearly all the potential markers of CR-CSCs so far proposed, such as CD133 [17, 18], CD44 [19], ESA (EpcAM) [18], CD166 [19], ALDH-1[9], Musashi 1 (Msi1) [20], and LGR5 [21] require staining and are not completely unique for the CSC population.

It is therefore highly desirable to develop an alternative, rapid, and reliable technique for CR-CSC detection and sorting. The identification of such a method could also reveal new relevant cellular/functional aspects of the CSC subpopulation [14]. Raman techniques have been recently used for biological and medical studies as they display, due to the sensitivity to the chemical structure of biomolecules, non-perturbative sampling capabilities, label-free imaging, and high spatial resolution [22–24]. For instance, Raman microspectroscopy has been used to study DNA and protein distribution inside cells [25, 26], the cellular uptake and distribution of liposomal drug carriers [27], label-free mitochondrial distribution [28], lipidomic in leukocytes [29], and lipid imaging in human lung-cancer cells and in brain tissues [30].

In this study, Raman spectroscopy, fluorescence microscopy, flow-cytometry, and electron microscopy are used to investigate the presence of distinctive features of CR-CSCs compared to differentiated tumor cells and normal epithelial colon cells. We show that Raman microspectroscopy highlights a higher content of lipids in CR-CSCs compared to the differentiated counterpart and normal CR cells. Fluorescence microscopy with hydrophobic dyes, BODIPY [31], and LD540 [32] clearly identifies the origin of the larger lipid content as an increased expression of lipid droplets (LDs). The large amount of LDs is also confirmed and quantified by flow cytometry and electron microscopy. As a remarkable point, we find that LD content in CSC subpopulation is directly correlated with the over-expression of CD133 and high Wnt/ β -catenin pathway activity, two well-accepted markers for CR-CSCs. The correlation between LD content and tumorigenic potential was checked through the injection of different subsets (LDs^{High}/LDs^{Low}) in NOD/SCID mice.

From a detection point of view, the large amount of LDs produces remarkable increased intensities of the Raman peaks corresponding to specific vibrations of fatty acids, and the intensity differences are so unambiguously evident that these Raman modes are ideal candidates as Raman markers for a fast, robust, and label-free method for CR-CSC identification. From a biological/functional point of view, LDs can be an ideal target for future colon cancer therapies.

MATERIALS AND METHODS

Cell Cultures

CR-CSC cultures were generated as previously described by Ricci-Vitiani *et al.* [6, 18] and cultured in ultra-low adhesion flasks (Corning, Lowell, MA, <http://www.corning.com>) in Dulbecco's modified Eagle's medium (DMEM)/F-12 serum-free medium (Life Technologies, Carlsbad, CA, <http://www.lifetechnologies.com>) supplemented with fresh epidermal growth factor (EGF) (20 ng/ml) and basic fibroblast growth factor (FGF) (10 ng/ml) (Sigma-Aldrich, St. Louis, MO, <http://www.sigmaaldrich.com>) to promote their growth. A GFP⁺ subculture was obtained by lentiviral transduction as previously described [6]. Differentiated cells (sphere-derived adherent cells [SDACs]) were obtained by dissociating CR-CSCs and culturing them in Dulbecco's modified medium supplemented with 10% fetal calf serum (FCS) in adherent conditions for at least 25 days. Normal epithelial colon cells (NECCs) (CCD841-CoN, Manassas, VA, www.atcc.org) and colon carcinoma cell (CCC) lines (HCT116 and RKO, Manassas, VA, www.atcc.org) were cultured in RPMI and α -MEM completed with 10% of fetal bovine serum (FBS) and 1% of P/S, respectively.

Raman Measurements

Raman microspectroscopy is carried out by means of a Renishaw InVia Raman microscope (Wotton Under Edge, UK, www.renishaw.com), equipped with a motorized stage for the laser-scanning of the sample. The excitation wavelength is 633 nm and the incident light is focused on the sample through an Olympus (Olympus Italia S.r.l., Segrate, Italy, www.olympus-europa.com) $\times 60/1.0$ NA water immersion objective. The laser power at the sample level is about 3 mW. A notch-filter is used to block the Rayleigh back-scattered light. Before

recording Raman measurements, the cells are passaged by trypsinization, washed three times with phosphate buffered saline (PBS), and then resuspended in the same buffer. During the measurements, CaF₂ slides are used as substrates because of their negligible Raman signal background.

For the imaging experiments, cells were scanned through the laser focus in a raster pattern with a typical step-size of 1 μ m. Raman spectra are recorded in the 800–3,200 cm⁻¹ range and the accumulation time is 5 seconds per each pixel. Subsequently, Raman images were created by plotting the integrated intensity of a specific Raman band as a function of position. Since different biomolecules exhibit different characteristic Raman bands, this technique allows for a label-free imaging of the spatial distribution of biomolecules inside the cell.

Confocal Microscopy

Fluorescence images have been collected using a Nikon A1 confocal-laser-scanning microscope (Tokyo, Japan, www.nikon.com) with a PlanApo $\times 60$ oil immersion objective with a 1.40 numerical aperture. In suspension live cells have been stained for LDs using BODIPY 493/503 (Molecular Probes, Invitrogen, Carlsbad, CA, <http://www.lifetechnologies.com>). BODIPY 493/503 was used at 1 μ g/ml. Cells were washed with PBS 1 \times and incubated with BODIPY 493/503 for 15 minutes at room temperature.

Flow Cytometry

All cells were collected from the flasks, washed with PBS 1 \times , and incubated with BODIPY 493/503 at 1 μ g/ml or LD540 at 0.1 μ g/ml for 15 and 10 minutes, respectively, at room temperature in the dark. CD133 was stained using an anti-CD133 antibody (MiltenyiBiotec, Bergisch Gladbach, Germany, <http://www.miltenyibiotec.com>) allophycocyanin (APC)-conjugated (Invitrogen, Carlsbad, CA, <http://www.lifetechnologies.com/nl/en/home/brands/invitrogen.html>). Stained cells were washed twice with PBS 1 \times and resuspended in the same solution. Samples were analyzed by FACS Aria II flow cytometer (BD Biosciences, San Jose, CA, www.bd.com). To allow for comparison of the different cell lines, gains for forward-scattering, side-scattering, and fluorescence photo multiplier tubes are kept the same on all the measurements.

Transmission Electron Microscopy Measurements

NECCs, CR-CSCs, SDACs, and CCCs were processed for transmission electron microscopy. The volume fraction of the cell occupied by LDs was estimated using point counting stereology techniques (for more details see Supporting Information Methods).

Cell Sorting

Two different CR-CSC lines bearing the TCF Optimal Promoter (TOP)-green fluorescent protein (GFP) construct were collected from the flasks and sorted for GFP^{High} and GFP^{Low} (both sorted fractions consist of approximately 11%–13% of the total GFP⁺ population), using a fluorescence-activated cell sorting (FACS) FACS Aria II, and then stained for LD content using the LD540 dye.

Limiting Dilution Assay

The self-renewal capacity of the CR-CSC LDs^{High} and LDs^{Low} was assayed by dissociation of colon cancer spheroids and plating cells at serial dilution (1, 2, 4, 8, 16, 32, 64, and 128

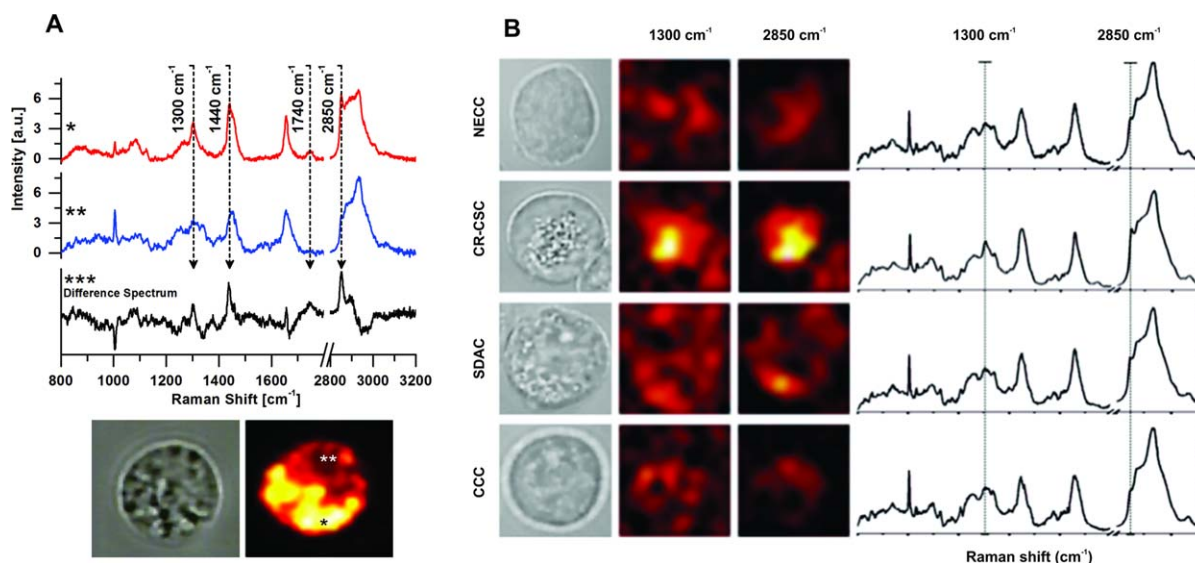


Figure 1. Raman characterization and mapping of colon cell samples. **(A):** Two different cell regions, indicated as * and **, respectively, can be clearly identified in the cell according to their Raman spectra. The Raman differences are due to four main peaks located at 1,300, 1,440, 1,740, and 2,850 cm^{-1} . Typical spectra from region * (top curve) and region ** (bottom curve) show that region * has higher expression of all these aforementioned peaks compared to region **, as clearly highlighted by the Raman difference spectrum ***; brightfield image of a CR-CSC and Raman imaging at 2,850 cm^{-1} of the same cell are reported, highlighting the two different regions. **(B):** From the top row to the bottom one: NECCs, CR-CSCs, SDACs, and CCCs. Brightfield images are reported on the first column, while Raman images calculated at 1,300 and 2,850 cm^{-1} are reported in the second and third column, respectively. The fourth column shows spectra averaged over the whole cell area, for each cell line. Raman images in the second column are similar to the corresponding ones of the third column, thus revealing that the two Raman modes at 1,300 and 2,850 cm^{-1} are space-correlated. Peaks related to lipidic vibrations are more pronounced in the CR-CSCs (second row) compared to SDACs and CCCs, as it is evident both from Raman images and spectra. NECCs reported in the first row express the lowest Raman intensities of lipidic vibrations. Abbreviations: CCC, colon carcinoma cell; CR-CSC, colorectal cancer stem cell; NECC, normal epithelial colon cell; SDAC, sphere-derived adherent cell.

cells per well) in 96-well microplate with flat bottom and repellent surface for low attachment (CELLSTAR Cell-Repellent Surface, Greiner Bio-One, UK, <http://www.selectscience.net/products/cellstar-cell-repellent-surface/?prodID=171921>). The cell culture medium used for this assay is the CSC medium described above (DMEM/F-12 serum-free medium, supplemented with fresh EGF and basic FGF). Results were statistically evaluated after 4 weeks using the Extreme Limiting Dilution Analysis (ELDA) software [33].

In Vivo Tumorigenicity Assay

Mice experiments were performed according to the animal care committee guidelines of the University of Palermo. For in vivo limiting-dilution injection, total CR-CSC population was sorted for LD540 intensity and 100, 500, 1,000, and 8,000 cells from 12% lowest and 12% highest were deposited by FACS in a 96-well plate containing stem cell medium, admixed with matrigel, and then injected subcutaneously in 5-week-old NOD/SCID mice (Charles River Laboratories, IT, <http://www.criver.com>). Tumor size was measured weekly using an electronic caliper and the volume was then calculated with the formula: larger diameter \times (smaller diameter)² \times $\pi/6$. At the end of the experiments, mice were sacrificed and tumors collected. Tumor tissues were finally processed for morphological and immune-histochemical analysis or for in vitro culture.

Statistical Analysis

Most of the Raman spectra presented in this work are average curves coming from a large number of measurements. Standard deviation and principal component analysis (for

more details see Supporting Information) were used for Raman analysis.

Transmission electron microscopy (TEM) comparison of the volume fraction of cell occupied by LDs for each sample was done with Student's *t* test (for more details see Supporting Information). For clonogenic assay, the statistical analysis was performed with Prism 5 (GraphPad Software, La Jolla, CA, <http://www.graphpad.com>) applying Bonferroni Multiple Comparison Test. Differences were considered significant with *p*-values $<.05$ (*) and $<.01$ (**).

RESULTS

CR-CSCs Show a Specific Lipid Raman Signature

Primary CR-CSC lines, characterized for CD133 [18] expression and high Wnt/ β -catenin pathway activity [6], and SDACs from distinct human CR cancer specimens derived from seven patients (stage II-IV) undergoing CR resection (see Supporting Information) were analyzed by Raman spectroscopy. In addition, NECCs and two CCCs were used for comparison. Figure 1A shows a typical Raman imaging result recorded on a single CR-CSC. When analyzing the spectra measured across the cell area, two spatial regions (named region * and **) with different Raman features were identified. The characteristic Raman spectra (Fig. 1A*, 1A**) from these regions exhibit clear differences for peak intensity at 1,300, 1,440, and 1,740 cm^{-1} and for the Raman band at 2,800–3,000 cm^{-1} . The assignment of all these Raman bands has been thoroughly discussed in literature, with the peaks at 1,300 and 1,740 cm^{-1}

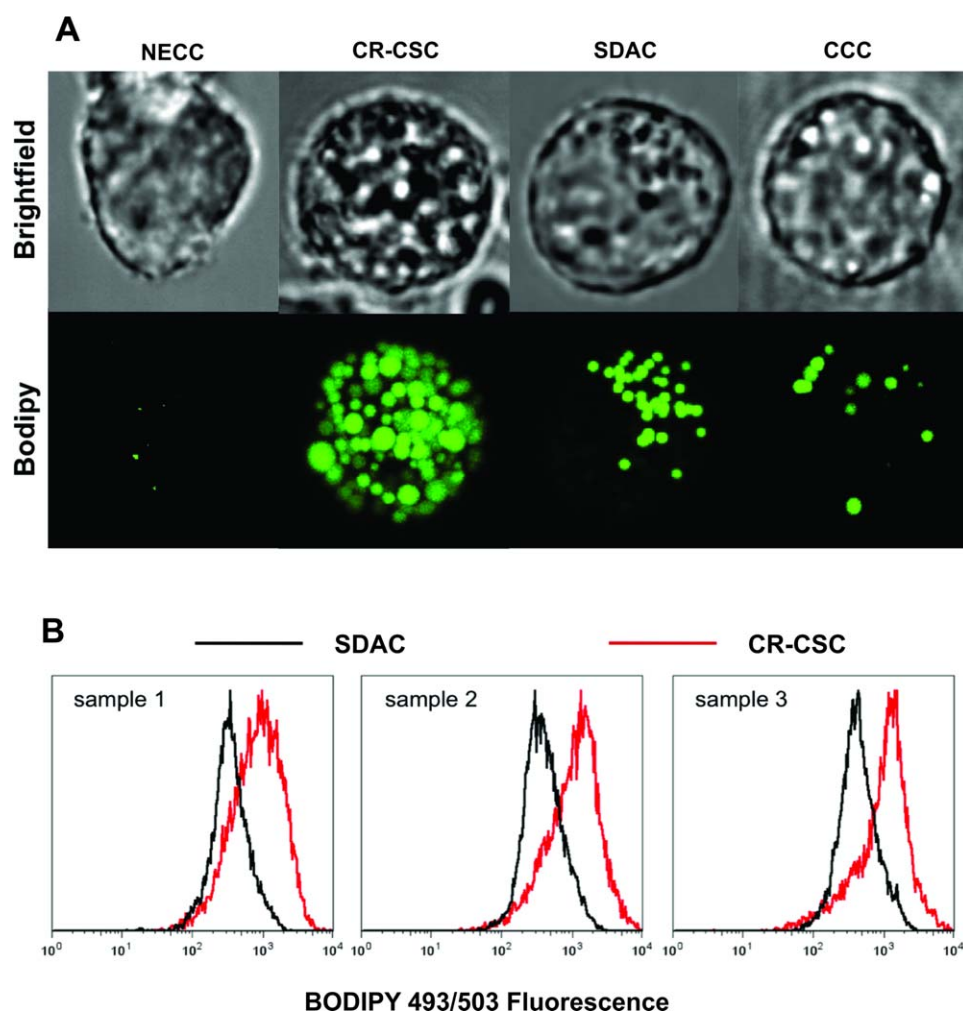


Figure 2. Lipid droplet quantification. **(A):** Comparison of typical z-projected confocal fluorescence images of the investigated cell lines stained with BODIPY 493/503. The lipid droplet content on CR-CSCs is higher compared to all the other cell lines. **(B):** Histograms overlay for flow-cytometry BODIPY fluorescence measurements regarding three of the CR-CSC (red) lines and their SDACs (black). Abbreviations: CCC, colon carcinoma cell; CR-CSC, colorectal cancer stem cell; NECC, normal epithelial colon cell; SDAC, sphere-derived adherent cell.

unambiguously assigned to molecular vibrations of lipids [34, 35], while the $1,440\text{--}1,450\text{ cm}^{-1}$ and $2,800\text{--}3,000\text{ cm}^{-1}$ bands are indicators for the lipid to protein ratio (see Supporting Information).

Comparison of the two spectra (Fig. 1A***) revealed that region * has a larger content of lipids. Besides the intensity increase observed for the peaks at $1,300$ and $1,740\text{ cm}^{-1}$, which are characteristic only of lipids, both the aforementioned lipid to protein indicators ($1,440\text{--}1,450$ and $2,800\text{--}3,000\text{ cm}^{-1}$ bands) denote larger lipid content. In fact, a detailed analysis of the $1,440\text{--}1,450\text{ cm}^{-1}$ band shows a shift toward the $1,440\text{ cm}^{-1}$ vibration typical of lipids, while in the $2,800\text{--}3,000\text{ cm}^{-1}$ region the CH_2 symmetric stretching at $2,850\text{ cm}^{-1}$ is noticeably more pronounced (CH_2 groups are more frequent in fatty acids than in proteins). Overlapping the bright-field image of the cell with the Raman map at $2,850\text{ cm}^{-1}$ clearly shows that these lipid-rich areas correspond to the presence of granulated (or droplet-like) morphological structures. Also, imaging at $1,300$, $1,440$, and $1,740\text{ cm}^{-1}$ (data not shown) exhibits the same spatial correlation with the bright-field image. These peaks are therefore

spatially overlapping, which confirmed the lipid nature of the observed droplets.

Figure 1B shows the typical Raman imaging for all the measured cell lines, with intensity maps at $1,300$ and $2,850\text{ cm}^{-1}$, along with whole-cell-averaged Raman spectra on the last column. CR-CSCs clearly exhibit a distinctive Raman signature with remarkable intensities for the two aforementioned peaks. Again, these features are localized in spatial regions corresponding to granules observed in the bright-field image of the cell. The SDACs have partially inherited this characteristic, but at a smaller extent. Even if some spots are still noticeable in the bright-field picture of the cell (mostly in the left-bottom part of the SDACs in Fig. 1B), the peaks intensities at $1,300$ and $2,850\text{ cm}^{-1}$, on the averaged Raman spectra, are much smaller compared to CR-CSCs. CCCs exhibit, instead, few spots. Accordingly, Raman intensities at $1,300$ and $2,850\text{ cm}^{-1}$ drop to smaller values, and Raman spectra from CCCs generally resemble to Raman profile of region ** of Figure 1A. Finally, the NECCs (first row in Fig. 1B) show the most uniform appearance, with a nearly absence of spots in the

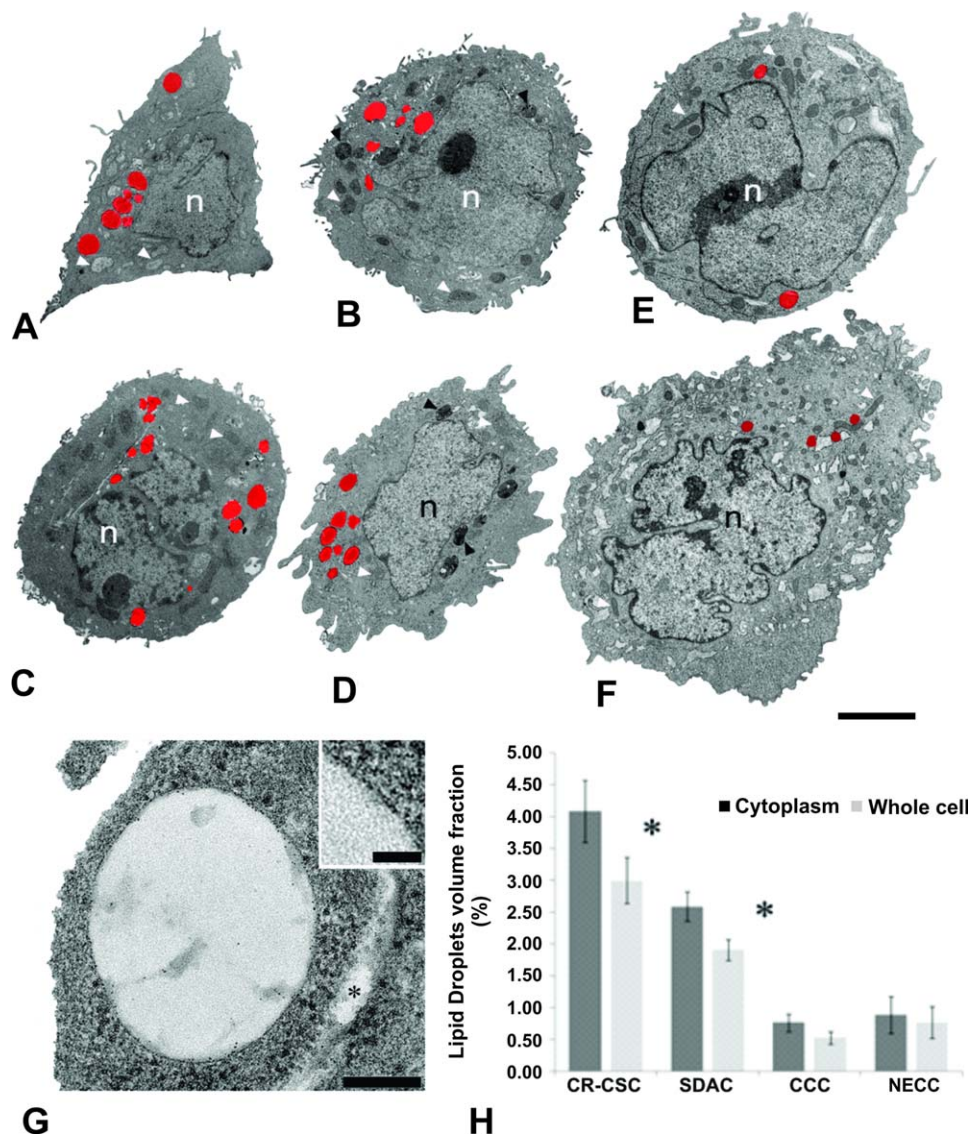


Figure 3. Transmission electron microscopy (TEM) to reveal lipid droplets on colorectal cells. **(A–F):** TEM images of the CR-CSCs, their differentiated forms (SDACs), CCCs, and NECCs. **(A and B)**, parasagittal sections of **(A)** CR-CSCs and **(B)** SDACs belonging to human patient 1; **(C and D)**, parasagittal sections of **(C)** CR-CSCs and **(D)** SDACs belonging to human patient 2; **(E)**, parasagittal section of a CCC; **(F)**, parasagittal section of a NECC. White arrowheads point to mitochondria; black arrowheads point to multivesicular bodies and late-endosome/lysosome hybrids. LDs are colored in red. n, nucleus. **(G):** TEM image of a LD in cross-section. The asterisk points to the endoplasmic reticulum. Inset: detail of the LD single membrane leaflet. **(H):** Volume fraction of LDs in the cytoplasm and in the whole cell. Error bars, SEM. Statistical significance is denoted by * ($p \leq .01$, Student's *t* test). Scale bars are 4 μm for A–F and 100 nm for G. Abbreviations: CCC, colon carcinoma cell; CR-CSC, colorectal cancer stem cell; NECC, normal epithelial colon cell; SDAC, sphere-derived adherent cell.

bright-field image, and also their Raman spectra have small intensities at the characteristic frequencies of lipids vibrations.

In order to prove that Raman spectroscopy can provide a fast tool for CR-CSC detection (and for future sorting applications) we extended our measurements. Besides point-by-point Raman mappings, we measured a single Raman spectrum in the 800–1,800 cm^{-1} range for each cell using a line-focused laser excitation extending for the whole cell diameter. In these measurements (see also Supporting Information Fig. S1, S2), the 1,300 cm^{-1} Raman peak of CR-CSCs displayed an intensity level that was much more pronounced than in normal cells or in other non-stem CR cancer cell

lines, suggesting that it can be used as a Raman marker for detecting CR-CSCs. We noticed that, due to the clear change in spectra between CR-CSCs and the other cell types, no data treatments were necessary (we reported Principal Component Analysis in Supporting Information Fig. S3 just to point out the sensitivity of the method [36]).

LD Quantification

To confirm the presence, and to assess the amount of the lipid-rich regions revealed by Raman spectroscopy, fluorescence imaging and flow cytometer measurements were performed on the cell samples using BODIPY 493/503 or LD540

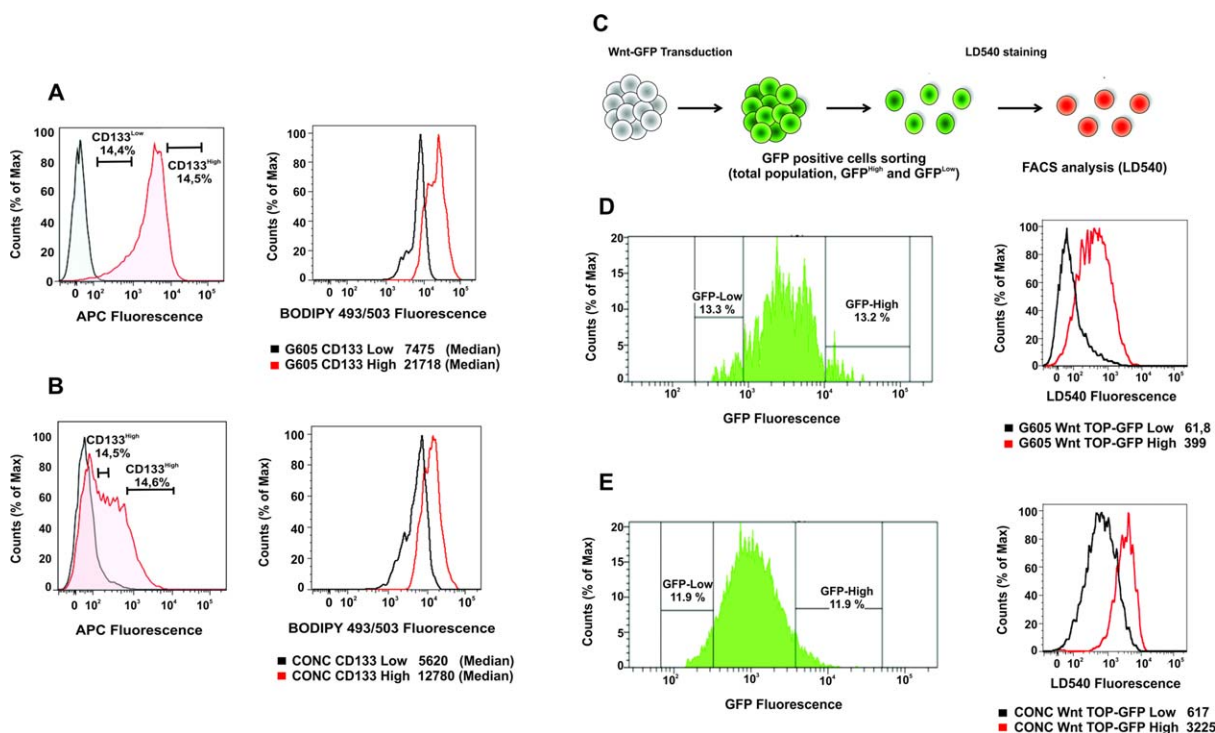


Figure 4. Correlation of the expression levels of the Lipid Droplets with CD133 and Wnt/ β -catenin. **(A, B):** The expression of the LDs in CD133^{High} and CD133^{Low} cells were analyzed by flow cytometry. Cells were stained with an anti-CD133 APC-conjugated and then with BODIPY 493/503. Both CD133^{High} samples (A and B red lines) have a higher expression of LDs compared to the CD133^{Low} (black lines). **(C):** Schematic representation of the TOP-GFP Wnt construct. **(D, E):** Cells were sorted for GFP expression (GFP^{High} and GFP^{Low}) and then stained for LDs with LD540 dye; both TOP-GFP samples have the same behavior showing as Wnt/ β -catenin pathway expression clearly correlates with LDs quantity. Abbreviations: APC, allophycocyanin; FACS, fluorescence-activated cell sorting; GFP, green fluorescent protein; TOP, TCF Optimal Promoter (TOP).

staining, which are consolidated dyes for cellular LD visualization [32, 37, 38].

Confocal images were collected for all the colon cell lines and z-projections created using the ImageJ software [39]. The acquired images clearly showed the “lipid droplet” nature of the same granular structures visible in the bright-field image, which are responsible for the high lipid-related Raman peaks. A comparison of typical LD content among the considered samples is shown in Figure 2A and Supporting Information Figure S4. From this it is clear that the number of LDs increases from the normal cells to the CR-CSCs.

Moreover, flow-cytometric analysis allows for a statistical assessment of the LD expression difference among the investigated cell lines. Comparison of histograms for CR-CSC lines from three different patients and their related SDACs confirmed the higher LD expression in multiple CR-CSCs.

The ultra-structural analysis performed with TEM on NECCs, two different CR-CSC samples, their relative SDACs, and CCCs, corroborated both Raman and fluorescent microscopy results (Fig. 3). The LDs were unambiguously identified in the cell cytoplasm, often close to the endoplasmic reticulum (Supporting Information Fig. S5), as subcellular structures delimited by a single membrane leaflet (Fig. 3G and inset) [37]. The stereological analysis, performed to quantify the volume fraction of the LDs in the various cell lines analyzed, further confirmed the insights from Raman and fluorescent microscopy (Fig. 3H). We measured a LD volume fraction expressed as percentage of cytoplasmic volume ranging from

$4.09\% \pm 0.48\%$, for the CR-CSCs, to $0.89\% \pm 0.29\%$, for the NECCs, value that fall into the range reported for other cell types (Fig. 3H) [40]. In the CR-CSCs, the LD volume fraction in the whole cell and in the cytoplasm resulted to be significantly higher ($p \leq .01$), compared to that measured for SDACs (Fig. 3H). Furthermore, the LD volume fraction in the SDACs was largely higher ($p \leq .01$) compared to that measured inside the NECCs and the CCCs (Fig. 3H).

Correlation Between CD133, Wnt, and LDs

To verify whether LD content and the expression of CR-CSC markers directly correlate, we performed flow cytometer measurements of CD133 expression and Wnt/ β -catenin pathway activity. In a first experiment, different CR-CSC samples were double-stained for LDs and CD133 with BODIPY 493/503 and anti-CD133 antibody. Flow cytometric analysis (Fig. 4A, 4B) showed a clear correlation between the two markers. In a second experiment, LDs and Wnt correlation was studied using two CR-CSC cultures with a TOP-GFP reporter gene [6]. Importantly, cells derived from these single-cell cloned TOP-GFP cultures still showed a big heterogeneity in Wnt signaling level [6]. The two cell lines were sorted based on the GFP fluorescence, as an indicator of Wnt activity, into two subsets, Wnt^{High} and Wnt^{Low}. Sorted cells were then stained for LD content using the LD540 dye, taking advantage of the fact that it can be used in combination with GFP (green) since its emission spectrum extends to red fluorescence (Fig. 4C–E). It

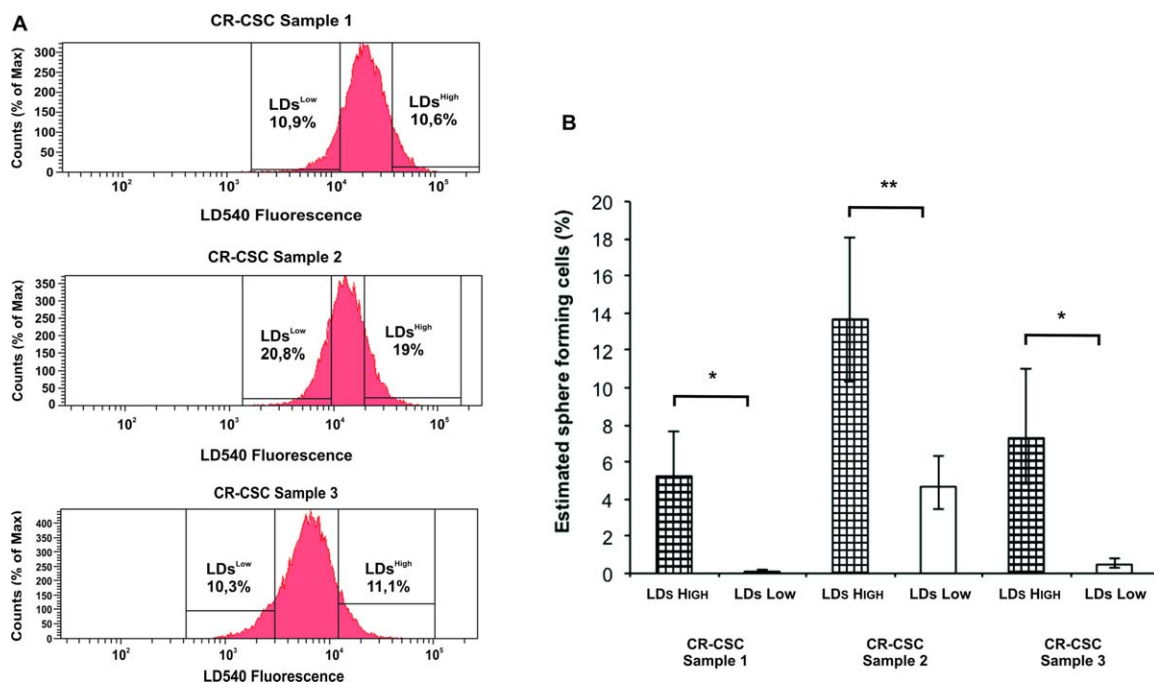


Figure 5. Clonogenic assay of CR-CSC LDs^{High/Low} subpopulations in vitro. Three different CR-CSC samples were tested for their clonogenic potential. **(A):** CR-CSCs were sorted for LDs^{High} and LDs^{Low} by fluorescence activated cell sorting for LDs using LD540 dye and then deposited 1, 2, 4, 8, 16, 32, 64, and 128 cells per well. **(B):** The estimated sphere-forming cells were analyzed using the extreme limiting dilution analysis as reported in the graph. All the three LDs^{High} cell samples have a significantly increased clonogenic potential compared to the LDs^{Low} cell samples. Error bars representing the SD of the mean of three independent experiments are shown. Significance is indicated (*, $p < .05$ and **, $p < .01$). Abbreviations: CR-CSC, colorectal cancer stem cell; LD, lipid droplet.

is evident that LD expression and Wnt signaling level strongly correlate. It is important to note that the different expression of LDs is not due to the use of different cell media, since Wnt^{High} and Wnt^{Low} cells were sorted from the same population, such as for the case of CD133, as reported above. These results, showing a clear correlation between CD133, Wnt, and LD content, indicate that LDs could be used as CR-CSC marker, and suggest a possible functional or metabolic link of LDs in CR-CSCs [41, 42].

A High LD Content Is Linked to Clonogenic Potential of CR-CSCs

Different CR-CSC lines were stained with the LD540 dye and sorted in LDs^{High} and LDs^{Low} populations. The sorted cells were used to perform a limiting dilution assay (LDA) to test the clonogenic potential. The results reported in Figure 5 show that LDs^{High} cells possess a higher clonogenic potential compared to the LDs^{Low} in all the CR-CSC lines analyzed, indicating that LD content correlates with clonogenicity. In addition, this may suggest a possible role of these LDs in giving an advantage in promoting and sustaining cell growth. These data show that CR cells contain a subpopulation of cells with high levels of LDs that can be used as a marker to single out the CSC subset present within heterogenic tumor cell population.

In Vivo Tumorigenic Potential Analysis

To determine whether CR-CSC LDs^{High} and LDs^{Low} fractions display tumorigenic potential, we injected CR cancer cells subcutaneously in immune-compromised mice. The experiment was performed using four different cellular dilutions (8,000,

1,000, 500, and 100 cells), for both LDs^{High} and LDs^{Low} fractions, and following the tumor growth over time after cells injection. Although both CR-CSC LDs^{High} and LDs^{Low} exhibited tumorigenic activity, LDs^{Low} cells generated delayed small tumors, whereas the LDs^{High} cell fraction was able to grow as large tumors (Fig. 6A, 6B). Such a low tumorigenic activity of the LDs^{Low} population was lost when a small number of cells (≤ 500 cells) were subcutaneously injected, suggesting that cells endowed with tumorigenic potential are included into the LDs^{High} population, while LDs^{Low} cells could represent the more differentiated nontumorigenic cell population (Fig. 6A). Of note, 17 weeks later, we observed that xenograft tumors recapitulated the morphological features of the parental CR tumors (Fig. 6C, 6D).

DISCUSSION

In the last years, it was shown that CR cancer cells exhibit more LDs than their normal counterpart [41, 43], but here we have found that CR-CSCs can be identified for having the largest amount of LDs when compared with differentiated tumor or normal epithelial cells. This finding has been confirmed by measurements carried out on CR-CSCs from seven different patients and a well-studied TOP-GFP reported gene cell system for Wnt/ β -catenin pathway activity [6]. We have demonstrated through an in vivo assay that, even though some CR-CSC LDs^{Low} could be tumorigenic and develop slowly growing small tumors, most of the tumorigenic potential is restricted to the CR-CSC LDs^{High} fraction.

We can speculate that the higher expression of LDs in CR-CSCs could be part of the disease pathogenesis confirming

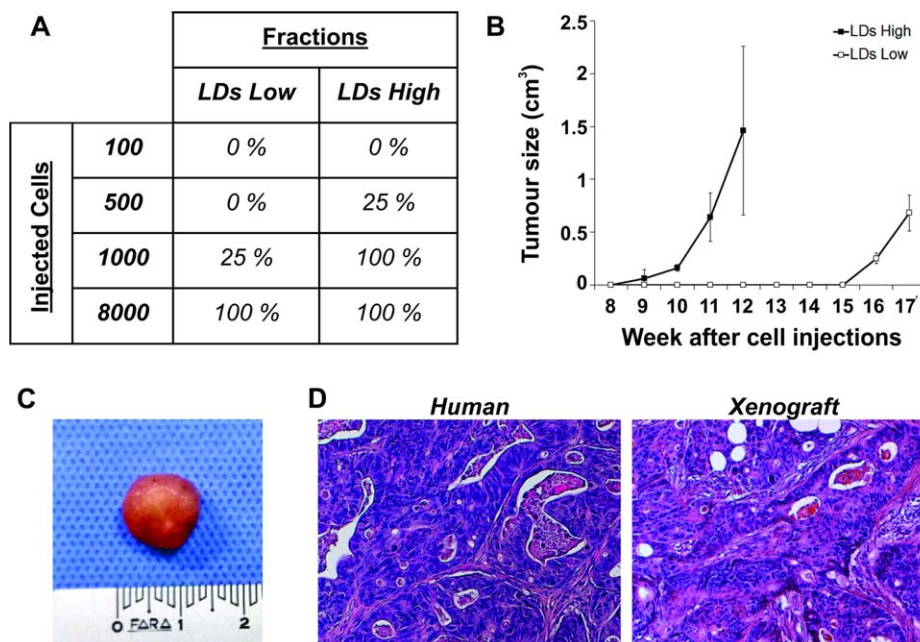


Figure 6. Cells with high lipid droplet content show cancer stem cell (CSC) tumorigenic features in vivo. **(A):** In vivo transfer of LD540 stained cultures. Different cell numbers from the indicated populations were injected into NOD/SCID mice after fluorescence-activated cell sorting. The percentage of successful tumor initiations after 17 weeks out of four injections for each condition is shown. The LDs^{High} fraction showed the highest tumor-initiating capacity (refer Fig. 6B for the kinetic of tumor appearance). **(B):** Time course of colon tumor growth after injection of 8,000 LDs^{High} or 8,000 LDs^{Low} CR-CSCs (tumor volumes were determined as described in Materials and Methods). **(C):** Representative picture of the xenotransplanted tumors. **(D):** Hematoxylin/eosin staining of xenografts shows clear evidence of colon carcinoma morphology, resembling the human parental phenotype. Abbreviation: LD, lipid droplet.

the increasing interest toward these organelles, shown by the recent literature [41, 42]. Even if LD role is not yet clear, there are evidences of the over-expression of these organelles in colon cancer development. LD accumulation was indeed found in polyp epithelium of Apc^{Min} mice, suggesting that they may contribute to polyp development [44].

It is known that LDs in neoplastic cells act as distinct intracellular domain for regulated eicosanoids production (Prostaglandin E2) starting from arachidonic acid (AA) [43]. The metabolism of AA is directly implicated in the generation of a chronic inflammatory tissue environment that could promote carcinogenesis. For instance, 80%–90% of colon carcinomas show an enhanced cyclooxygenase-2 (COX-2; prostaglandin H synthase) expression compared with normal intestinal mucosa [45–47]. COX-2 is the enzyme that catalyzes the rate-limiting step in eicosanoids synthesis, converting AA into prostaglandins. Our results could therefore point to a potential link between LDs over-expressing CR-CSCs and inflammation in cancer.

Additionally, besides their function in the generation of eicosanoids, LDs constitute sites of compartmentalization of several signaling-relevant proteins, which may have functions beyond AA metabolism. Indeed, proteins with well-established roles in oncogenic cell transformation, tumorigenesis, and metastasis, or identified as potential CR cancer biomarkers including PI3K, ERK2, p38, PKC, caveolin, and ADRP, were shown to localize in LDs in a variety of cell types [48–51].

Although no specific LD inhibitors have been described so far, different classes of drugs have been demonstrated to inhibit diverse lipid pathways, both in a direct or indirect way; some of them, such as nonsteroidal anti-inflammatory drugs

[52, 53] and statins [54] could interfere with LD formation in vitro and in vivo. Even if the mechanism of action of these drugs is not completely understood, they have exhibited successful results in the prevention of the CR cancer, suggesting a pivotal role for the LDs in CR-CSCs. Moreover, very recent results are indicating an even tighter connection between lipid metabolism and stemness [55, 56].

The biological implications of LD overexpression in CR-CSCs need further investigations. On this side, we could just speculate that the higher content of LDs may be crucial for CR-CSCs in giving them an advantage in proliferation [57], as an energy reserve to resist starvation, to survive in prohibitive microenvironment conditions (oxidative/energy stress), or even stimulating signaling pathways promoting cell invasion [58].

In this work, we also propose a new method, Raman spectroscopy, to highlight and characterize CR cancer stemness. While, at the moment, there are no procedures available for clinical use based on this label-free technique, a quick look to the recent scientific literature shows that pivotal achievements on the technical side have been accomplished [59, 60] and we believe that a clear track has been traced to make it an effective tool in clinical diagnosis. Differently from label-based fluorescence analysis, the Raman technique collects the whole spectral content without any additional tagging procedure, and without any external perturbation of the cell biological machinery, becoming ideal for in vivo multimolecular detection. It is worth noticing that several research groups are working to develop high sensitivity Raman-based microendoscopes for future in vivo screening [59, 60]. These technical achievements, combined with our finding about the abundance of LDs (that are an ideal target for Raman

detection) in CR-CSCs, place a solid ground to our view that a Raman clinical application is reasonably within the reach.

CONCLUSIONS

Our data put in evidence that LDs could be considered as new and important “players” in CR-CSCs, and a rather interesting cellular target for future innovative anticancer therapies. Moreover, we propose identification of CR-CSCs through Raman spectroscopy, a label-free technique, able to visualize the LD cell content.

ACKNOWLEDGMENTS

We thank Ennio Albanesi for technical help in flow-cytometry measurements, Francesco Paonessa and Daniele Di Mascolo for help in cell staining, Luigi Atzori, Giovanni Morrone and Francesco Trapasso for useful discussions. Simone Di Franco thanks the Ph.D. Programme in Immunopharmacology at the University of Palermo. This work was supported by grants from Associazione Italiana per la Ricerca sul Cancro to E.C. (AIRC IG 10189), G.S. (AIRC IG 8730 and AIRC 5x1000), and M.T. (AIRC IG 10254). L.P. and J.P.M. were supported by a grant of the National Fund against Cancer (SNFK) and Dutch Cancer Society Grants (UvA2009-4416 and UvA2012-5425).

REFERENCES

- Jemal A, Siegel R, Ward E et al. Cancer statistics, 2006. *CA Cancer J Clin* 2006;56:106–130.
- Schwitalla S, Fingerle AA, Cammareri P et al. Intestinal tumorigenesis initiated by dedifferentiation and acquisition of stem-cell-like properties. *Cell* 2013;152:25–38.
- Barker N, van Es JH, Kuipers J et al. Identification of stem cells in small intestine and colon by marker gene *Lgr5*. *Nature* 2007;449:1003–1007.
- Sneddon JB, Werb Z. Location, location, location: The cancer stem cell niche. *Cell Stem Cell* 2007;1:607–611.
- Visvader J. Cells of origin in cancer. *Nature* 2011;469:314–322.
- Vermeulen L, De Sousa E Melo, van der Heijden M et al. Wnt activity defines colon cancer stem cells and is regulated by the microenvironment. *Nat Cell Biol* 2010;12:468–476.
- Prasetyanti PR, Zimmerlin CD, Bots M et al. Regulation of stem cell self-renewal and differentiation by Wnt and Notch are conserved throughout the adenoma-carcinoma sequence in the colon. *Mol Cancer* 2013;12.
- Dieter SM, Ball CR, Hoffmann CM et al. Distinct types of tumor-initiating cells form human colon cancer tumors and metastases. *Cell Stem Cell* 2011;9:357–365.
- Todaro M. Colon cancer stem cells: Promise of targeted therapy. *Gastroenterology* 2010;138:2151–2162.
- Todaro M, Alea Mileidys Perez, Di Stefano AB et al. Colon cancer stem cells dictate tumor growth and resist cell death by production of interleukin-4. *Cell Stem Cell* 2007;1:389–402.
- Clarke MF, Fuller M. Stem cells and cancer: Two faces of eve. *Cell* 2006;124:1111–1115.
- Lathia J, Venere M, Rao M et al. Seeing is believing: Are cancer stem cells the Loch Ness monster of tumor biology? *Stem Cell Rev Rep* 2011;7:227–237.
- Shackleton M, Quintana E, Fearon ER et al. Heterogeneity in cancer: Cancer stem cells versus clonal evolution. *Cell* 2009;138:822–829.
- Medema JP. Cancer stem cells: The challenges ahead. *Nat Cell Biol* 2013;15:338–344.
- Clarke MF, Dick JE, Dirks PB et al. Cancer stem cells—Perspectives on current status and future directions: AACR Workshop on cancer stem cells. *Cancer Res* 2006;66:9339–9344.
- Ladman AJ, Martinez AO. Cell contacts and surface-features of 3 murine tumors grown as multicellular spheroids. *Eur J Cell Biol* 1988;45:224–229.
- O’Brien CA, Pollett A, Gallinger S et al. A human colon cancer cell capable of initiating tumour growth in immunodeficient mice. *Nature* 2007;445:106–110.
- Ricci-Vitiani L, Lombardi DG, Pilozzi E et al. Identification and expansion of human colon-cancer-initiating cells. *Nature* 2007;445:111–115.
- Dalerba P, Dylla SJ, Park IK et al. Phenotypic characterization of human colorectal cancer stem cells. *Proc Natl Acad Sci USA* 2007;104:10158–10163.
- Glazer RI, Vo DT, Penalva LOF, Musashi1: An RBP with versatile functions in normal and cancer stem cells. *Front Biosci (Landmark Ed)* 2012;17:54–64.
- Schepers AG, Snippert HJ, Stange DE et al. Lineage tracing reveals *Lgr5+* stem cell activity in mouse intestinal adenomas. *Science* 2012;337:730–735.
- De Angelis F, Das G, Candeloro P et al. Nanoscale chemical mapping using three-dimensional adiabatic compression of surface plasmon polaritons. *Nat Nanotechnol* 2011;5:67–72.
- De Angelis F, Gentile F, Mecarini F et al. Breaking the diffusion limit with superhydrophobic delivery of molecules to plasmonic nanofocusing SERS structures. *Nat Photon* 2011;5:683–688.
- Cottat M, Thioune N, Gabudean AM et al. Localized surface plasmon resonance (LSPR) biosensor for the protein detection. *Plasmonics* 2013;8:699–704.
- Das G, La Rocca R, Lakshminanth T et al. Monitoring human leukocyte antigen class I molecules by micro-Raman spectroscopy at single-cell level. *J Biomed Opt* 2010;15:027007.
- Uzunbajakava N, Lenferink A, Kraan Y et al. Nonresonant confocal Raman imaging of DNA and protein distribution in apoptotic cells. *Biophys J* 2003;84:3968–3981.
- Matthaeus C, Kale A, Chernenko T et al. New ways of imaging uptake and intracellular fate of liposomal drug carrier systems inside individual cells, based on Raman microscopy. *Mol Pharm* 2008;5:287–293.
- Matthaus C, Chernenko T, Tatyana N et al. Label-free detection of mitochondrial distribution in cells by nonresonant Raman microspectroscopy. *Biophys J* 2007;93:668–673.
- van Manen HJ, Kraan YM, Roos D et al. Single-cell Raman and fluorescence microscopy reveal the association of lipid bodies with phagosomes in leukocytes. *Proc Natl Acad Sci USA* 2005;102:10159–10164.

AUTHOR CONTRIBUTIONS

L.T., C.L., S.D.F., and P.C.: conception and design, collection and/or assembly of data, data analysis and interpretation, and manuscript writing; R.L.R., L.P., R.M., R.R., A.F., M.M., A.B., and F.D.A.: collection and/or assembly of data; V.P.R.: provision of study material or patient; M.T.: financial support, administrative support, provision of study materials or patients, collection and/or assembly of data, and final approval of manuscript; E.C.: conception and design, financial support, manuscript writing, and final approval of manuscript; J.P.M.: conception and design, financial support, administrative support, provision of study materials or patients, manuscript writing, and final approval of manuscript; G.S.: financial support, administrative support, provision of study materials or patients, manuscript writing, final approval of manuscript; E.D.F.: conception and design, financial support, administrative support, provision of study material or patients, data analysis and interpretation, manuscript writing, and final approval of manuscript. L.T., C.L., S.D.F., G.S., and E.D.F. contributed equally to this article.

DISCLOSURE OF POTENTIAL CONFLICTS OF INTEREST

The authors indicate no potential conflicts of interest.

- 30** Freudiger CW, Min W, Saar BG et al. Label-free biomedical imaging with high sensitivity by stimulated Raman scattering microscopy. *Science* 2008;322:1857–1861.
- 31** Listenberger LL, Brown DA. Fluorescent detection of lipid droplets and associated proteins. In: Juan S. Bonifacino, et al., eds. *Current Protocols in Cell Biology*/Editorial Board. Chapter 24, 2007:Unit 24 2.
- 32** Spandl J, White DJ, Peychl J et al. Live cell multicolor imaging of lipid droplets with a new dye, LD540. *Traffic* 2009;10:1579–1584.
- 33** Hu YF, Smyth GK. ELDA: Extreme limiting dilution analysis for comparing depleted and enriched populations in stem cell and other assays. *J Immunol Methods* 2009;347:70–78.
- 34** Chan JW, Motton D, Rutledge JC et al. Raman spectroscopic analysis of biochemical changes in individual triglyceride-rich lipoproteins in the pre- and postprandial state. *Anal Chem* 2005;77:5870–5876.
- 35** Wu H, Volponi JV, Oliver AE et al. In vivo lipidomics using single-cell Raman spectroscopy. *Proc Natl Acad Sci USA* 2011;108:3809–3814.
- 36** Candeloro P, Grande E, Raimondo R et al. Raman database of amino acids solutions: A critical study of extended multiplicative signal correction. *Analyst* 2013;138:7331–7340.
- 37** Martin S, Parton RG. Lipid droplets: A unified view of a dynamic organelle. *Nat Rev Mol Cell Biol* 2006;7:373–378.
- 38** Goodman JM. Demonstrated and inferred metabolism associated with cytosolic lipid droplets. *J Lipid Res* 2009;50:2148–2156.
- 39** Schneider CA, Rasband WS, Eliceiri KW. NIH Image to ImageJ: 25 years of image analysis. *Nat Methods* 2012;9:671–675.
- 40** Dees JH, Gazouli M, Papadopoulos V. Effect of mono-ethylhexyl phthalate on MA-10 Leydig tumor cells. *Reprod Toxicol* 2001;15:171–187.
- 41** Bozza PT, Viola JPB. Lipid droplets in inflammation and cancer. *Prostaglandins Leukot Essent Fatty Acids* 2010;82:243–250.
- 42** Farese RV, Jr., Walther TC. Lipid droplets finally get a little R-E-S-P-E-C-T. *Cell* 2009;139:855–860.
- 43** Accioly MT, Pacheco P, Maya-Monteiro CM et al. Lipid bodies are reservoirs of cyclooxygenase-2 and sites of prostaglandin-E-2 synthesis in colon cancer cells. *Cancer Res* 2008;68:1732–1740.
- 44** Mutoh M, Komiya M, Teraoka N et al. Overexpression of low-density lipoprotein receptor and lipid accumulation in intestinal polyps in Min mice. *Int J Cancer* 2009;125:2505–2510.
- 45** Eberhart CE, Coffey RJ, Radhika A et al. Up-regulation of cyclooxygenase-2 gene-expression in human colorectal adenomas and adenocarcinomas. *Gastroenterology* 1994;107:1183–1188.
- 46** Kargman SL, Oneill GP, Vickers PJ et al. Expression of prostaglandin G/H synthase-1 and synthase-2 protein in human colon-cancer. *Cancer Res* 1995;55:2556–2559.
- 47** Sano H, Kawahito Y, Wilder RL et al. Expression of cyclooxygenase-1 and cyclooxygenase-2 in human colorectal-cancer. *Cancer Res* 1995;55:3785–3789.
- 48** Fujimoto T, Kogo H, Ishiguro K et al. Caevolin-2 is targeted to lipid droplets, a new “membrane domain” in the cell. *J Cell Biol* 2001;152:1079–1085.
- 49** Pol A, Luetterforst R, Lindsay M et al. A caveolin dominant negative mutant associates with lipid bodies and induces intracellular cholesterol imbalance. *J Cell Biol* 2001;152:1057–1070.
- 50** Yu W, Cassara J, Weller PF. Phosphatidylinositol 3-kinase localizes to cytoplasmic lipid bodies in human polymorphonuclear leukocytes and other myeloid-derived cells. *Blood* 2000;95:1078–1085.
- 51** Matsubara J, Honda K, Ono M et al. Identification of adipophilin as a potential plasma biomarker for colorectal cancer using label-free quantitative mass spectrometry and protein microarray. *Cancer Epidemiol Biomarkers Prev* 2011;20:2195–2203.
- 52** Thun MJ, Henley SJ, Patrono C. Nonsteroidal anti-inflammatory drugs as anticancer agents: Mechanistic, pharmacologic, and clinical issues. *J Natl Cancer Inst* 2002;94:252–266.
- 53** Thun MJ, Jacobs EJ, Patrono C. The role of aspirin in cancer prevention. *Nature reviews. Clin Oncol* 2012;9:259–267.
- 54** Ali R, Toh HC, Chia WK et al. The utility of Aspirin in dukes C and high risk dukes B colorectal cancer - The ASCOLT study: Study protocol for a randomized controlled trial. *Trials* 2011;12:261.
- 55** Ito K, Suda T. Metabolic requirements for the maintenance of self-renewing stem cells. *Nat Rev Mol Cell Biol* 2014;15:243–256.
- 56** Sorrentino G, Ruggeri N, Specchia V et al. Metabolic control of YAP and TAZ by the mevalonate pathway. *Nat Cell Biol* 2014;16:357–366.
- 57** Francescangeli F, Patrizii M, Signore M et al. Proliferation state and polo-like kinase1 dependence of tumorigenic colon cancer cells. *STEM CELLS* 2012;30:1819–1830.
- 58** Santos CR, Schulze A. Lipid metabolism in cancer. *FEBS J* 2012;279:2610–2623.
- 59** Ji MB, Orringer DA, Freudiger CW et al. Rapid, label-free detection of brain tumors with stimulated raman scattering microscopy. *Sci Transl Med* 2013;5.
- 60** Saar BG, Johnston RS, Freudiger CW et al. Coherent Raman scanning fiber endoscopy. *Opt Lett* 2011;36:2396–2398.



See www.StemCells.com for supporting information available online.